Investigations of a boxed rotor: The STAR II rotor in DLR's test hall.

Gunther Wilke[AS]
Hideaki Sugawara[JX], Yasudata Tanabe[JX]
Oliver Schneider[FT], and Berend G. van der Wall[FT]

[AS] German Aerospace Center (DLR), Aerodynamics and Flow Technology[DLR]
[JX] Japan Aerospace Exploration Agency (JAXA), Osawa 6-13-1, Mitaka, Tokyo, 181-0015 Japan
[FT] German Aerospace Center (DLR), Flight Systems[DLR]
[DLR] Lilienthalplatz 7, 38108 Braunschweig, Germany

Abstract

The second Smart Twisting Active Rotor (STAR II) project aims at investigating active twist on a conventional blade design in the DNW-LLF wind tunnel. Prior to the wind tunnel test, the rotor is first tested for correct operation in the rotor test hall at the German Aerospace Center (DLR) in Braunschweig. This test shall ensure that all the instrumentation, but also the active twist, works correctly along with setting up the tracking of the blades before shipping the whole test setup to the DNW-LLF wind tunnel. From previous rotor tests in this hall, it was observed that vibration levels increased drastically above certain thrusts. Since there were no PIV tests carried out within this test chamber, it was decided to carry out CFD simulations to obtain visualizations of the flow and to find the origins of these vibrations. The rotor test hall was approximated by a simple box. With the help of CFD simulations carried out by DLR and JAXA, the initial guess of potential recirculation could be confirmed. The recirculation effect and vibrations become stronger with increasing thrust and therefore limits the maximum thrust in the test hall. This paper details the results of the CFD simulation and presents them along with initial experimental data from the rotor test hall.

Keywords: STAR II rotor, rotor in pre-test chamber, hover

1 Introduction

In anticipation of the upcoming wind tunnel test of the STAR II rotor [1] in the German-Dutch Wind Tunnels' Large Low-Speed Facility (DNW-LLF), the rotor and instrumentation is tested beforehand in the rotor test hall at the DLR in Braunschweig. The test hall is only of limited space and therefore the rotor is not only operated in-ground effect, but also re-circulation occurs. As in previous tests oscillations were observed, prior CFD simulations were carried out to investigate the impact on the operation within the test hall. The simulation results are compared against the experimental data. A glimpse of the experimental runs is given in Fig. 1.

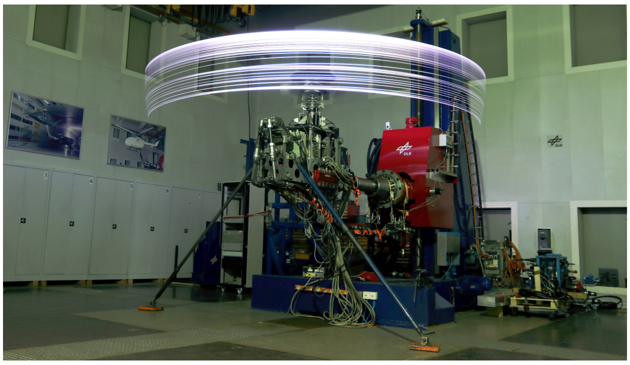

Figure 1: STAR II rotor during testing.

2 Literature Review

The in-ground effect of hovering rotors has long been studied experimentally as well as numerically and many more in free hovering flight.

Among the first numerical studies, Cheeseman and Bennett [2] formulate simple relations based on momentum theory. They already manage to recover the common observations that a hovering rotor in ground requires less power for the same thrust. Using potential theory, Heyson derives a model to compute the flow of a helicopter within the ground effect. Graber et al. [3] modify a free-wake model to investigate a rotor in ground. Johnson [4] also includes an in-ground analysis in his comprehensive code CAMRAD. The comprehensive code HOST is extended by Basset et al. [5] to include the in-ground effect in hover. Ananthan et al. [6] model the in ground effect in their free-wake model through a mirrored image rotor and also investigate the effect of vortex stretching within the wake. Tritschler et al. [7] apply a time-accurate free-wake method including a particle solver to mitigate the brownout effect of a rotor landing in a sandy environment. [8] Quackenbush et al. also validate their CHARM code to model the in-ground effect.

The S76 model rotor is analyzed in hover within and outside the ground effect by Balch and Lombardi [9]. With their experimental work, they confirm the numerical investigations that the required power becomes lower for the same thrust. Tanner et al. [10] look at the outwash wall-jet of the rotor in-ground-effect. They find that the jet velocities may become twice as large as the induced hover velocity of the rotor. Gibertini et al. [11] look at a model rotor nearing an obstacle on the ground. Applying their backward-oriented-Schlieren technique, Schwarz et al. [12] visualize the wake of a Bo-105 helicopter at full scale. Wolf et al. [13] utilize this system to also look at a H-145 helicopter and compare its measurements with repeated measurements of the Bo-105. They observe different vortex pairing behavior between these helicopters.

Kutz et al. [14], [15] validate their CFD based approach with measurements of a free-flying model helicopter. Their CFD approach includes structural deformations and a trim procedure to match the experimental data. Boisard [16] computes the test case from Gibertini et al. [11] and compares a free-wake method against a CFD based approach. He concludes that most cases could already be well replicated by the free-wake model, however, when re-ingestion was given in the experiment, the model failed to accurately predict this effect. Miesner et al. [17] look at a multi-copter configuration using CFD and find that the power reducing in-ground effect for this system is not observed as it is for a single main rotor system due to the increased interaction between these rotors. Similarly, Tanabe et al. [18] observed a changed in-ground effect for their drone in comparison to the existing conventional helicopter observations.

So far, only JAXA has carried out a simulation of a rotor in a test hall when investigating a helicopter for the Martian environment [19], [20], but DLR has had no experience in these simulations, yet. This paper focuses on a classical helicopter rotor in boxed flow. From Boisard [16] and JAXA's experience, it is deducted that the occurring recirculation needs to be captured with CFD. While potential based methods like free-wake methods maybe extended with source/sink terms to model the hall, their semi-empirical wake aging methods are likely more erroneous for this case than existing CFD methods.

3 Methodology

The general test setup is sketched in Fig. 2, which is a simplification of the actual experiment, compare Fig. 1. The test hall itself is not meant to replace the wind tunnel test, but to test out the blades under centrifugal forces alongside the test instrumentation. The goal of this pre-test is to ensure a well working setup before going to the real wind tunnel and fix potential faults drastically reducing wind tunnel costs. However, in previous pre-tests, certain oscillations are observed. In order to understand these better, while also lacking PIV measurements, it was decided to simulate the flow within the testing chamber and compare this with the free-stream results as they have been produced previously in [1].

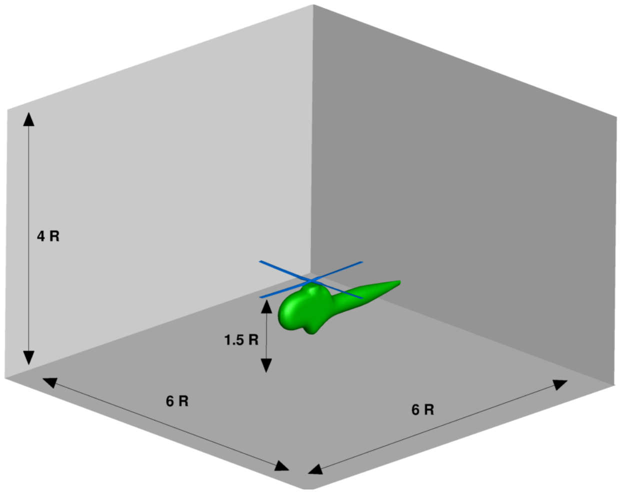

Figure 2: Sketch of rotor test setup in the testing facility.

JAXA and DLR offered to run these lengthy simulations. The working assumption is a closed box. A fully periodical solution is not expected, since the temperature will rise simply due to the power fed into the rotor. Nevertheless, the effect is assumed to be little, yet a drift is therefore expected in the results. On the JAXA side, the flow solver rFlow3D is utilized [21], whereas on the DLR side the flow solver FLOWer [22] is applied. Both codes use the SLAU2 scheme [23] with a slight modification for moving grids for the computation of the convective fluxes. The upwind flow states are reconstructed with the Fourth-order Compact MUSCL Transformation [24]. JAXA utilizes the original version, yet DLR has exchanged the Minmod limiter with a van Albada type limiter [25] to further enhance accuracy. Regarding turbulence modelling, JAXA relies on a fully turbulent simulation with the Menter SST model [26], while DLR applies empirical transition predictions [27] to the SA-DDES-R turbulence model variant [28], [29], [30]. The time-stepping is done using a dual-time stepping approach [31] for the whole domain on DLR side, whereas JAXA only applies this method to the geometry grids. In the background, an explicit fourth order Runge Kutta scheme is utilized. Both results are fluid-structural coupled. DLR uses Airbus Helicopters' HOST code [32] using the delta air loads approach, JAXA it's in-house rMode code. For the boxed flow, the viscous wall boundary condition is applied, whereas for the out-of-ground simulations, also referred to as free simulations, DLR uses the Froude boundary condition, while JAXA applies the simple far field boundary condition with significantly extended boundaries to avoid reflections.

The grids are detailed below. Since only little knowledge is given on this type of simulations, the partners had slightly different philosophies in their simulation strategies. DLR choose to couple the last quarter

case	boxed		free	
partner	DLR	JAXA	DLR	JAXA
$\Delta\psi$	0.5^o	0.1^o	0.5^o	0.1^o
blade cells				
chord	128	141	128	141
span	128	157	128	157
normal	64	71	64	71
boundary layer	20	25	20	25
total blade	1 M	1.5M	1 M	1.5 M
fuselage cells	1 M	-	1 M	-
background grid				
$\Delta x/c_{ref}$	14%	20%	14%	20%
total bg	55 M	91M	69M	107M
total sim.	60 M	97M	74 M	113M

Table 1: Grid Metrics.

revolution after five revolutions at each coupling step, whereas JAXA coupled every half revolution. DLR's philosophy is to let the flow develop first and then couple, whereas JAXA's approach mimics more a tight coupling approach. Regarding the grid strategy, DLR focused on resolving the wake and vortices, whereas JAXA decided to also resolve the test hall wall boundary layer correctly. A cut through the respective test hall grids including the rotor is shown in Fig. 3 and in Fig. 4 for out-of-ground simulations. Their respective cell counts and according time steps are documented in Table 1. DLR included the fuselage as it would be used in the wind tunnel, however, in the test hall, the cover has been removed for practical reasons. Nevertheless, the main effect of the fuselage is its displacement effect, which should still be given, even without the cover. The background grid spacing $\Delta x/c_{ref}$ refers to the background grid resolution in the vicinity of the rotor. For DLR, this is halved in the remaining test chamber and outside the wake stream for the out-of-ground simulation. For JAXA, the outer grid becomes finer again near the walls, to capture the higher gradient of the velocity in the in-ground-effect and assuming this creeping up at the walls. Their estimation is $0.05m$ above the ground, where the outwash jet reaches its highest velocity and spent 5 points for the wall boundary layer. Initially, DLR started out with a grid $1/8$ in cell count, where every other grid point has been skipped and time step enlarged, to quickly gain insight into the problem as less computational resources are required. This setup will be referred to as 'coarse', whereas the other setup will be the 'fine' solution.

4 Results

Since the rotor test hall itself is not a wind tunnel, but a confined space, the thrust is usually limited by occurring recirculation, starting around $2,000N$ for the rotors given here. Two thrusts were therefore chosen to be simulated, one at $2,000N; c_T/\sigma = 3.54/100$ and one at $3,600N; c_T/\sigma = 6.37/100$, which corresponds to the set design weight. The operational conditions along with metrics of the rotor are listed in Table 2. The rotor in the simulations is also trimmed for zero moments, while this was ignored during the runs in the test hall. As will be seen later, the impact is little, but the reason for imposing this in the simulations is to spot any asymmetry more easily. The momentum theory is used to estimate the induced flow velocity of $8.1m/s$ for the $2,000N$ case, and then the time for a particle travelling with this velocity the distance from the rotor to the ground, to the walls, to the top of the hall and back to the center and down to the rotor plane, basically half the circumferential distance of $20m$, corresponds to roughly $2.5s$ or 43 revolutions. Assuming that 1-2 passes are necessary to have the circulation going, the simulations were carried out up to 100 revolutions. For the higher thrust case, the revolutions for a pass reduces to 32 revolutions. This is a very crude assumption, but as will be seen later, the magnitude of revolutions is in a fair standing and thus a

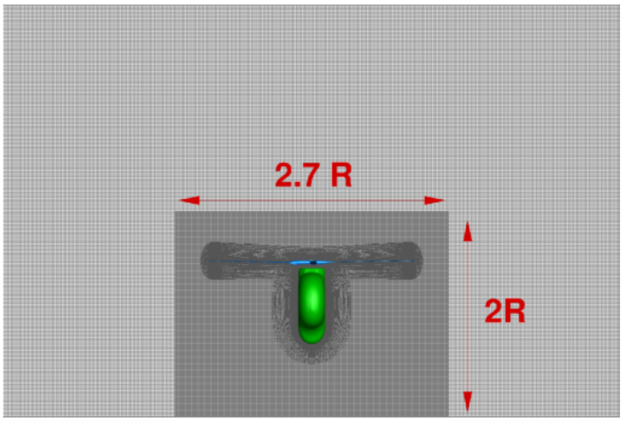

(a) DLR fine

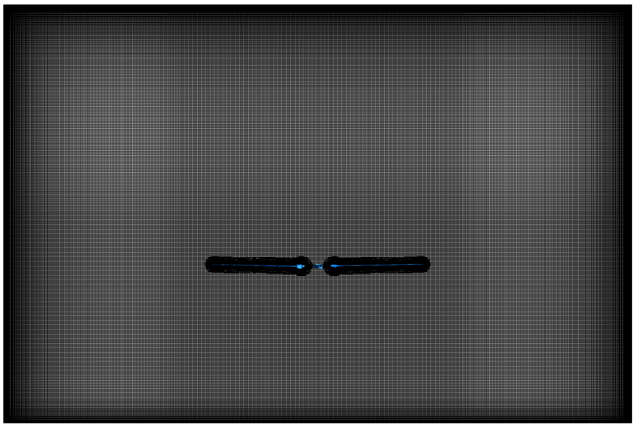

(b) JAXA

Figure 3: Boxed, hover in test hall grids.

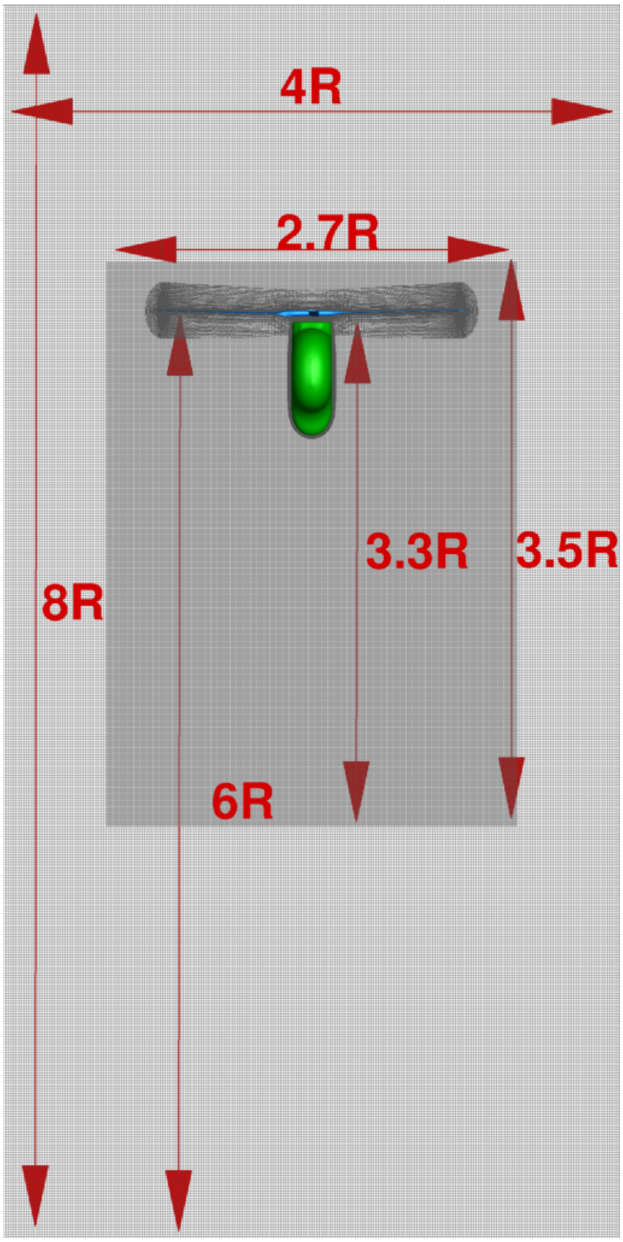

(a) DLR fine

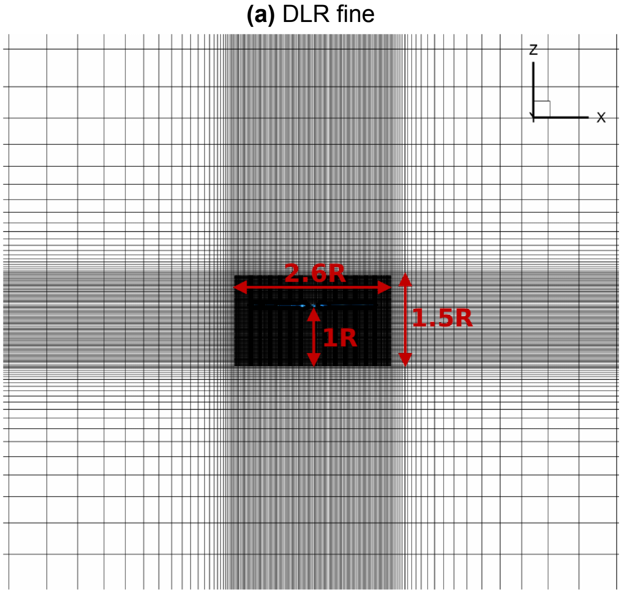

(b) JAXA

Figure 4: Free, hover out of ground grids.

lot larger than for regular rotor simulations in forward flight, where $10-20$ revolutions usually suffice in total depending on the flight condition.

parameter	value
Radius R	$2m$
chord c	$0.121m$
twist $\theta(r)$	$-8^o(r/R-0.75)$
solidity σ	0.077
airfoil	NACA23012 with tab
RPM	1042
M_{tip}	0.64
density ρ	$1.226kg/m^3$
temperature T	288.15^o K
trim goals	roll & pitching moment zero at set thrust
thrusts	$(2000, 3600)N$
c_T	$(2.72, 4.91)/1000$
c_T/σ	$(3.54, 6.37)/100$
trim variables	$\theta_0, \theta_c, \theta_s$

Table 2: Rotor specifications and (initial) operational condition.

In Fig. 5 and Fig. 6, the evolution of the collective pitch angle and the required power are plotted over the number of revolutions for the $c_T/\sigma = 3.54/100$ and $c_T/\sigma = 6.37/100$ cases in boxed and free operations. For the DLR simulations, only every 5 revolutions a coupling step is performed to have the flow settle in-between coupling steps, whereas JAXA coupled every half revolution. From these plots it is seen that the free flight condition converges more quickly than the boxed flow simulations. For JAXA with the tighter coupling every half revolution, this occurs roughly after 30 revolutions and for DLR after 40 revolutions for the free flow simulations. As expected, the boxed flow simulations do not fully converge, but the recirculation is established after 60-70 revolutions for the lower thrust and around 45-55 revolutions for the higher thrust simulations. Again, the JAXA results converge faster due to the tighter coupling. The common observation is that when the initial wake hits the ground, the collective is slightly lower than for the free flight simulations. Then the recirculation starts to develop and the collective pitch values start to grow and eventually surpass the free flight values as the climb effect from the recirculation outweighs the inground effect. Also, the boxed flow simulations start to oscillate in their global values when recirculation occurs. These fluctuations are greater for the higher thrust case. The coarse DLR grid shows the expected drift of variables more than the other two simulations, which however seems to be also an issue with too much inherent numerical dissipation. The DLR fine grid shows a strong kink for the boxed flow. Some stability issues where encountered on the comprehensive code side and changes were made on the fly to alleviate these instead restarting the simulation from scratch. Due to the lengthy runtimes of these simulations (in excess of 3 months), it was decided to continue them instead of restarting them. The DLR fine grid simulation of the free flight had to be restarted from scratch and therefore has not reached as many revolutions as the other simulations. It is still accepted, as this data point is at the higher thrust and in the free flow, where, when comparing with the coarse grid setup, convergence of the forces is quickly reached.

To gain more understanding of the flow within the box, the vertical velocity as well as the vorticity are plotted in Fig. 7 for the $c_T/\sigma = 3.54/100$ case and in Fig. 8 for the $c_T/\sigma = 6.37/100$ case. On a broad perspective, the flow fields between DLR and JAXA look similar, the core stream shows peak velocities downwards, which are then deflected to the side and almost with the same intensity moving up at the bounding walls. The stream tube contraction for the out-of-ground hover is not given, but the stream tube widens as part of the in-ground effect of the rotor. Similarly, to the velocity distribution, the vorticity and the tip vortices travel downstream and roll on the ground towards the walls and then up before they diffuse. The reason why the DLR simulations show more secondary vortices as well as a more jagged vertical velocity distribution is that outside the blade grids, the DDES method transitions into LES mode, whereas JAXA utilized plain U-RANS simulations which then show more of an averaged flow with mostly the primary/tip vortices left. Despite these differences, these higher frequency content seems to play a secondary role. While in the U-RANS simulation, those vortices will be represented by turbulent viscosity, in case of the DDES simulation, these fluctuations will be resolved and lead to the same result, the diffusion of the primary tip vortices and wake. Another difference observed is the upwash in the center of the rotor head in the JAXA simulations versus a purer inflow for the DLR simulation. The reason is that in the DLR simulation, the blades are tied together in the middle to form a proxy hub and therefore suppress this upwash mostly along with the included fuselage.

In Fig. 9 and Fig. 10 the corresponding flow fields for the free, out-of-ground, hovering rotor simulations are depicted for both thrusts. For brevity, only the DLR fields are shown. The JAXA results look similar with the exception that the secondary vortices are less as already observed for the boxed flow. In both cases, the flow appears well established and sufficiently converged downstream with the initial vortex pushed sufficiently away. For the DLR simulations, the outer farfield is depicted as well. Minor artifacts are observed; however, they are outside the refined boxed and are likely not changing the result significantly. From the out-of-ground perspective, which may be assumed for a helicopter past three rotor diameters, even placing the wall boundary condition instead of the Froude boundary condition should not have a large impact if the flow can exit side-ways. Also, no reflections are observed at the hanging grid nodes, only the resolution is lowered and blurs the picture more. The stream tube contraction is seen a bit better for the higher thrust case. For the lower thrust, the wake breaks down due to the meandering of the primary tip vortices and decomposition into smaller secondary appears relatively close to the rotor, and therefore the contraction is more difficult to see.

Moving from the flow field observations to the comparison with the available data of the wind tunnel, the collective pitch angle and the Figure of Merit are compared to the experiment in Fig. 11. The cyclic pitch angles, are not plotted for brevity and have not been used during the test. They remain below 0.15^o for the boxed and free flow for both simulations and are larger for the DLR simulations. Since they are of the same magnitude for the boxed and free simulation, the asymmetry is assumed to be given from the fuselage rather than from the box. In contrast, for JAXA the cyclic control angles remained below 0.05^o and are rather (numerical) noise than true moment adjustments. Investigating the collective pitch control angles, the correlation with the experiment is in good agreement with the simulations tending to require higher angles for the same thrust as the experiment. The free simulations require less collective for the same thrust, as they do not suffer from the recirculation. The Figure of Merit plots are generally in good agreement with the experiment. JAXA is slightly below the Figure of Merit of the experiment as is even further the solution of the DLR fine grid. The boxed flow on the DLR coarse grid yields reasonable results and follows the Figure of Merit curve of the experiment albeit with an offset to lower values. The agreement between the fine and coarse grid is also in good standing for the free flow. The lower Figure of Merit over the other results is argued with the lower grid resolution leading to an inherently higher numerical dissipation. The employed higher order deteriorates within in the boundary layer, where highly stretched cells are given and the lower order metric becomes crucial. However, for the flow within the test hall, but also in the free flow wake, the 4th order can be reached as the metric remains of high quality on the Cartesian mesh. The trend, that the free simulations require a smaller collective pitch angle and arrive at a better Figure of Merit than their boxed counterparts is given for both partners and grid densities. In the rotor test hall, the design thrust has not been investigated due to too severe oscillations and the maximum thrust has been $T = 3,420N; c_T/\sigma = 6.23/100$, slightly below the simulations.

Going into further detail, the sectional normal forces

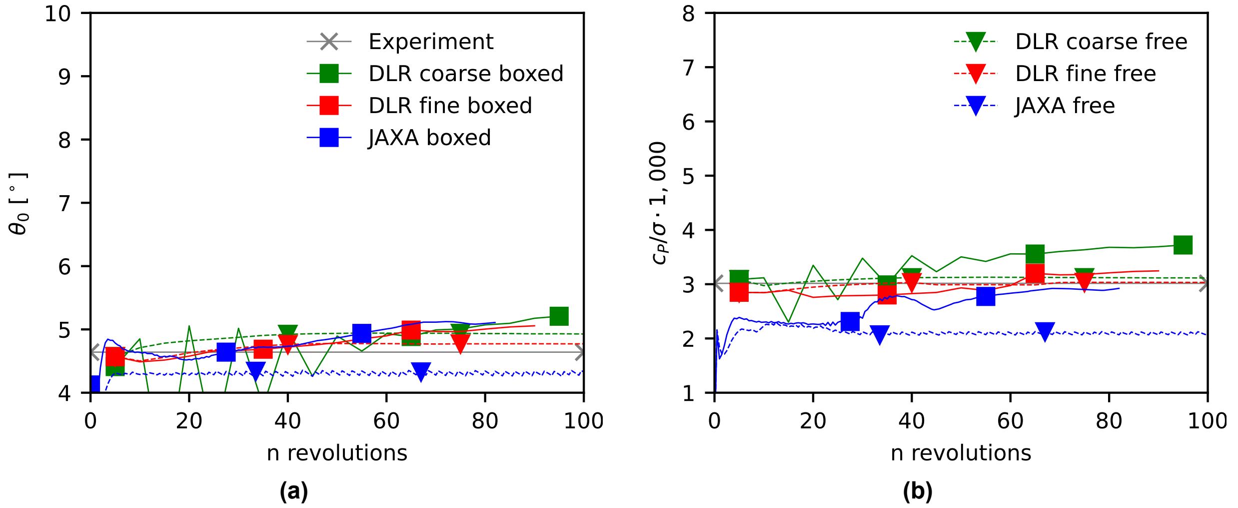

Figure 5: Evolution of the global values for the $c_T/\sigma = 3.54/100$ case.

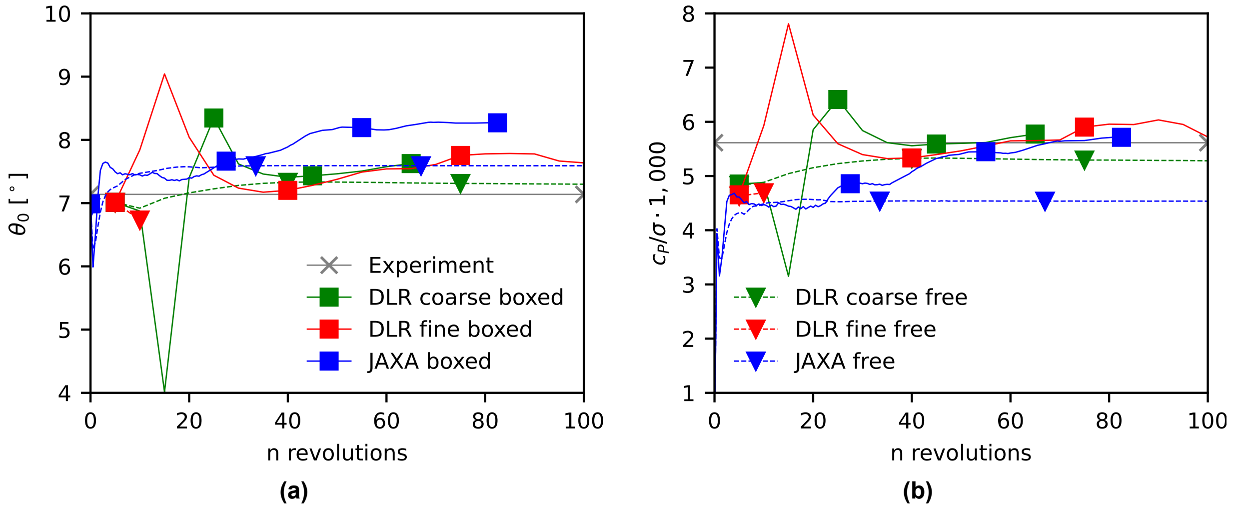

Figure 6: Evolution of the global values for the $c_T/\sigma = 6.37/100$ case.

are compared among the partners in Fig. 12 for the boxed and in Fig. 13 for the free simulations. For the DLR coarse grid simulations, the tip vortex peak is generally less pronounced and most pronounced for the DLR fine simulation. The peak is also reduced for the boxed flow cases over the free flow cases as the tip vortex of the preceding blade is already pushed further below the rotor due to the recirculation than for the free flight simulation. The doubled standard deviation, representing the 95% interval, marked by the slim lines is little for the free flow simulations, but is noticeably larger for the boxed flow simulations. Especially, at the higher thrust condition, the variation in normal force becomes quite significant, also an indicator for vibrations and likely the explanation why this thrust could not be safely investigated anymore in the rotor test hall.

5 Summary

From the shown results, it becomes apparent that the boxed flow of the rotor in the test hall is

1. High unsteadiness and oscillations in the global forces occur. The in-ground effect is observed in the flow fields; however, especially at higher thrusts, the recirculation dominates the final result as the power requirements of the rotor increased over the free flight condition.

2. The free flight condition at the moderate thrust shows less of the stream tube contraction. The bursting of the tip vortices and interaction with the wake lead to a practical finite length of the stream tube.

3. The delta airloads approach may not be suited for the boxed flow simulation. However, on a practical level, in the test hall, the collective was set

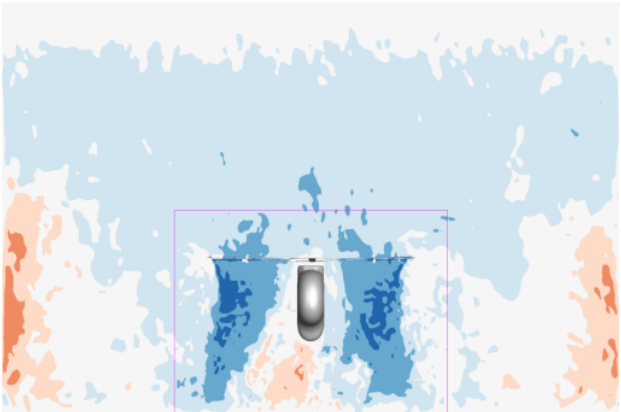

(a) vertical velocity - DLR fine grid

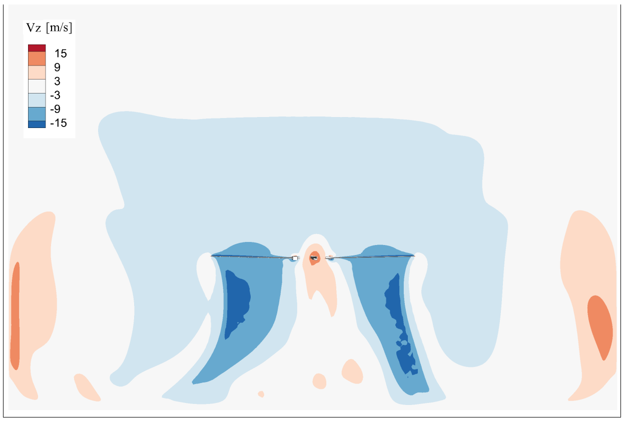

(b) vertical velocity - JAXA

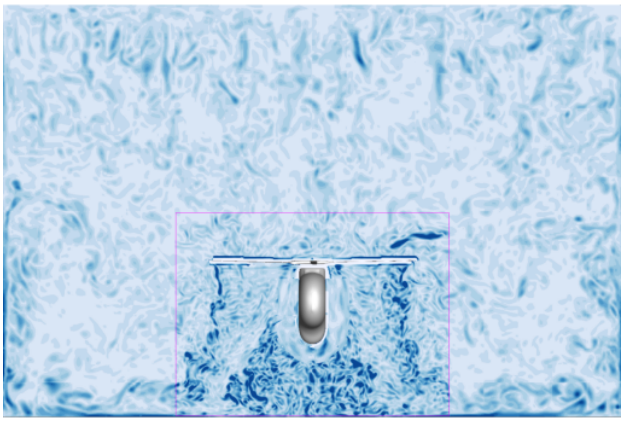

(c) vortex - DLR fine grid

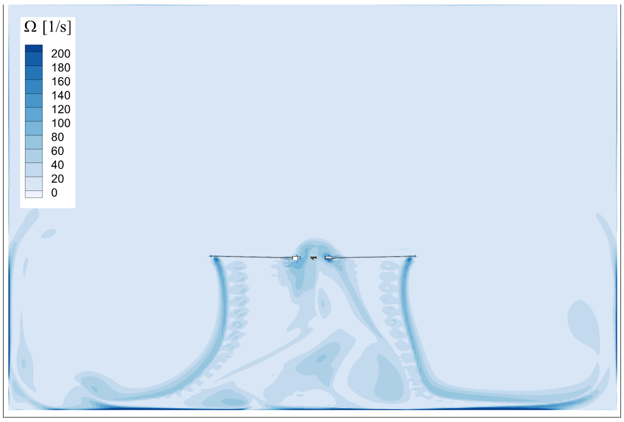

(d) vortex - JAXA

Figure 7: Boxed flow field for at a $c_T/\sigma = 3.54/100$. Same scales used.

(a) vertical velocity - DLR fine grid

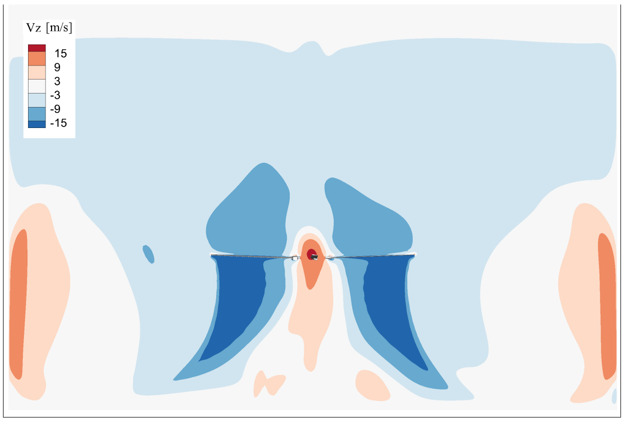

(b) vertical velocity - JAXA

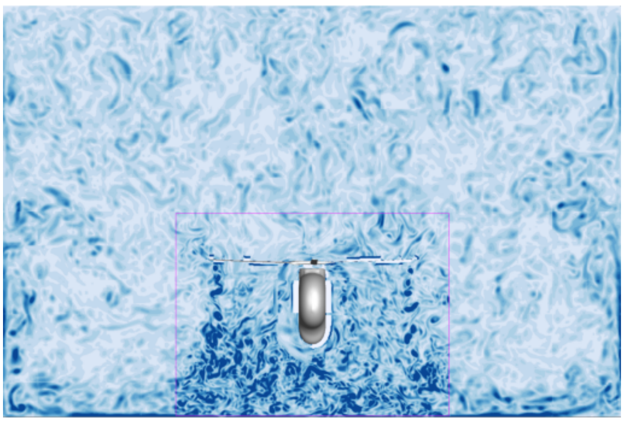

(c) vortex - DLR fine grid

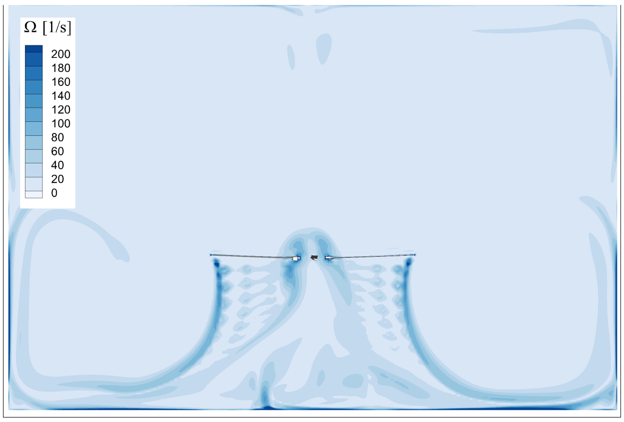

(d) vortex - JAXA

Figure 8: Boxed flow field for a thrust of $c_T/\sigma = 6.37/100$.

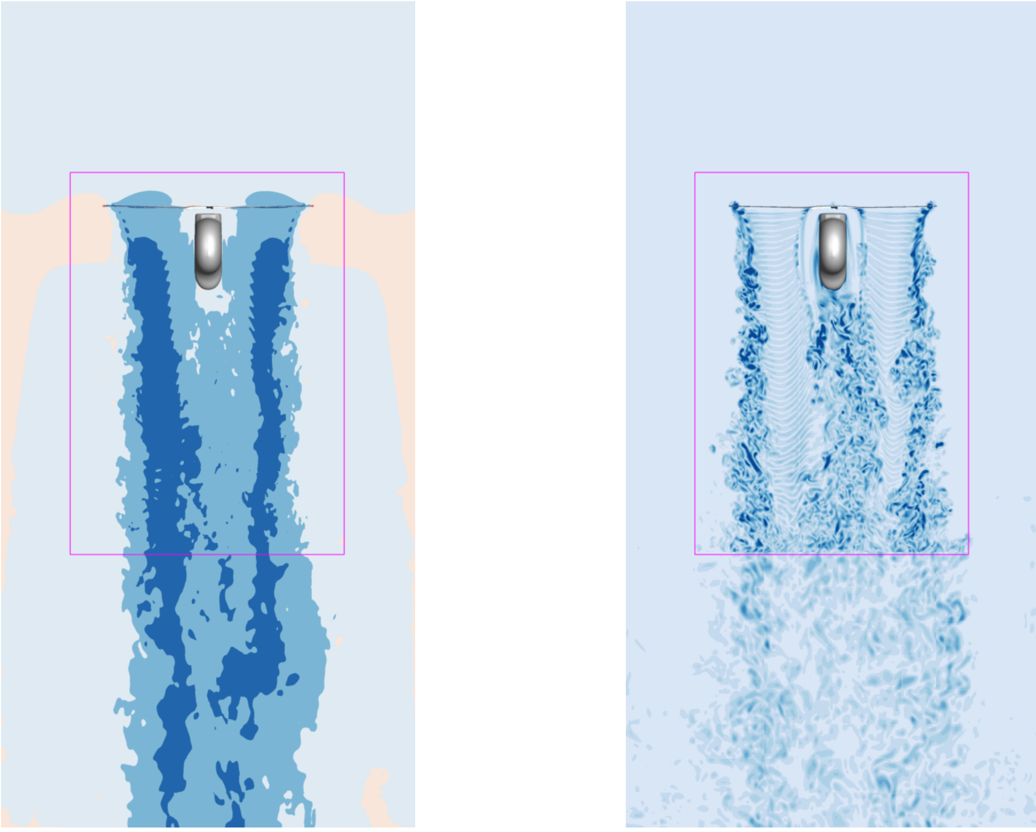

(a) vertical velocity - DLR fine grid

(b) vorticity - DLR fine grid

Figure 9: Free flow field for at a $c_T/\sigma = 3.54/100$.

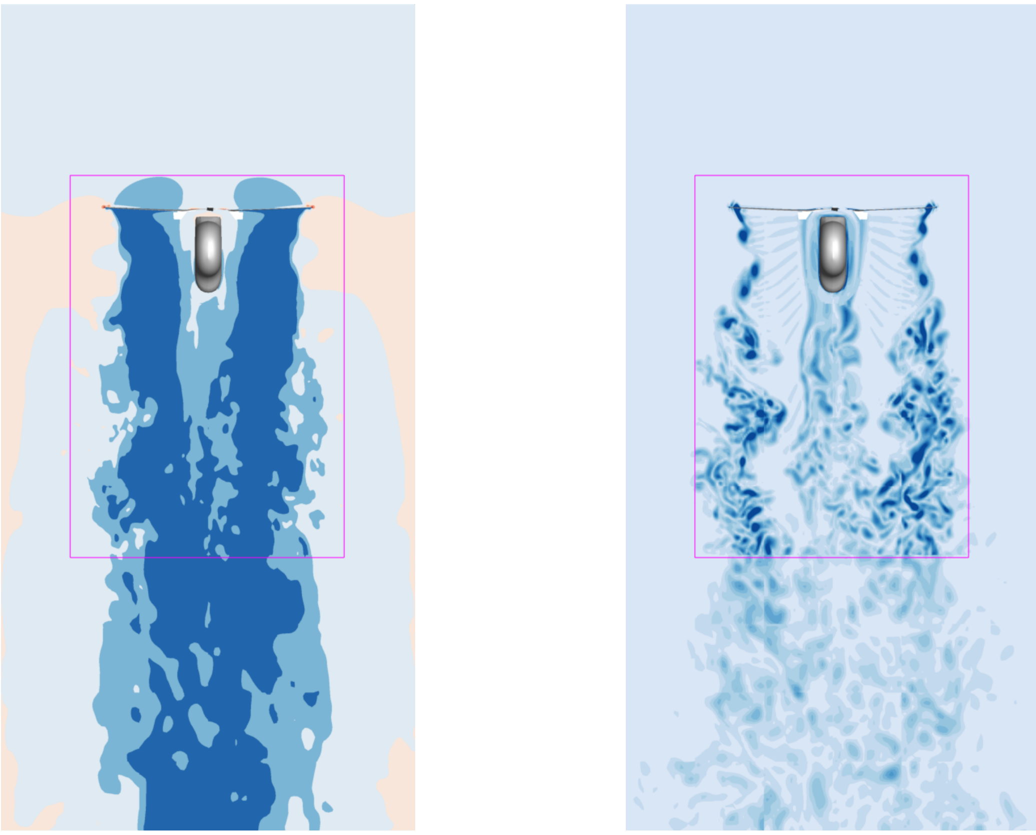

(a) vertical velocity - DLR coarse grid

(b) vorticity - DLR coarse grid

Figure 10: Free flow field for at a $c_T/\sigma = 6.37/100$.

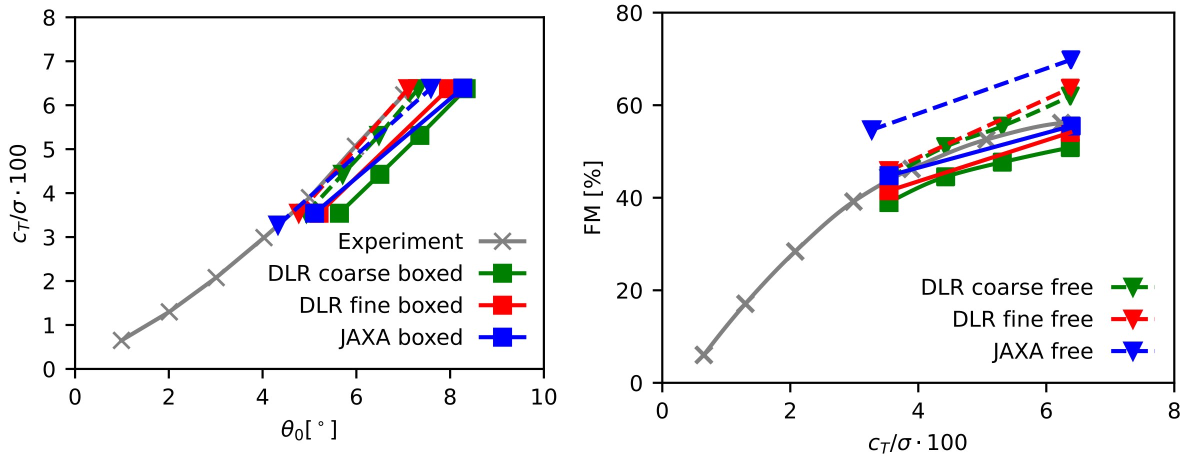

(a) Thrust over collective pitch angle

(b) Figure of Merit over thrust

Figure 11: Comparison of collective pitch angle, thrust and Figure of Merit with Experiment.

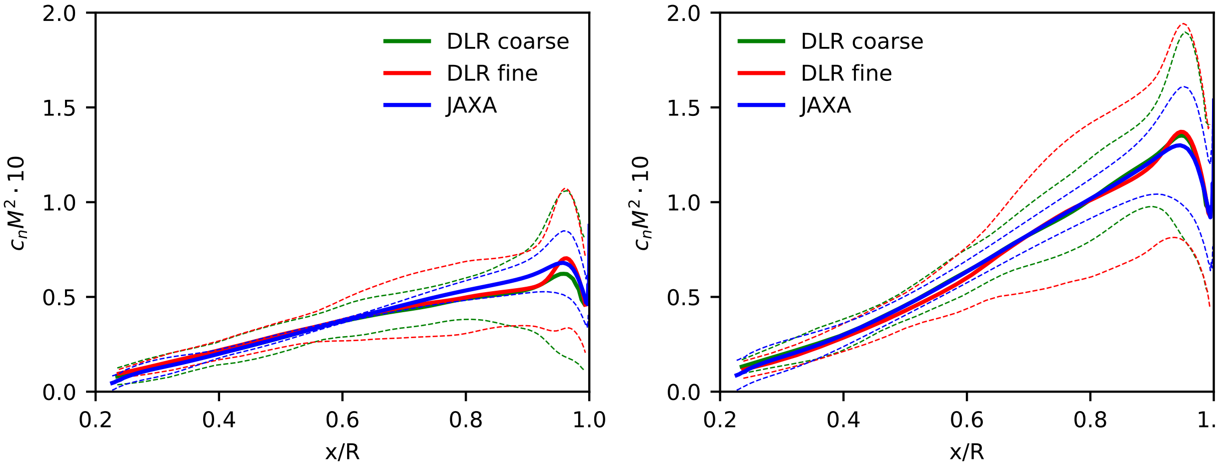

(a) $c_T/\sigma = 3.54/100$

(b) $c_T/\sigma = 6.37/100$

Figure 12: Normal force coefficients from the boxed simulations. The slim dashed lines show 2 standard deviations/95% interval added to the mean force with the thick line.

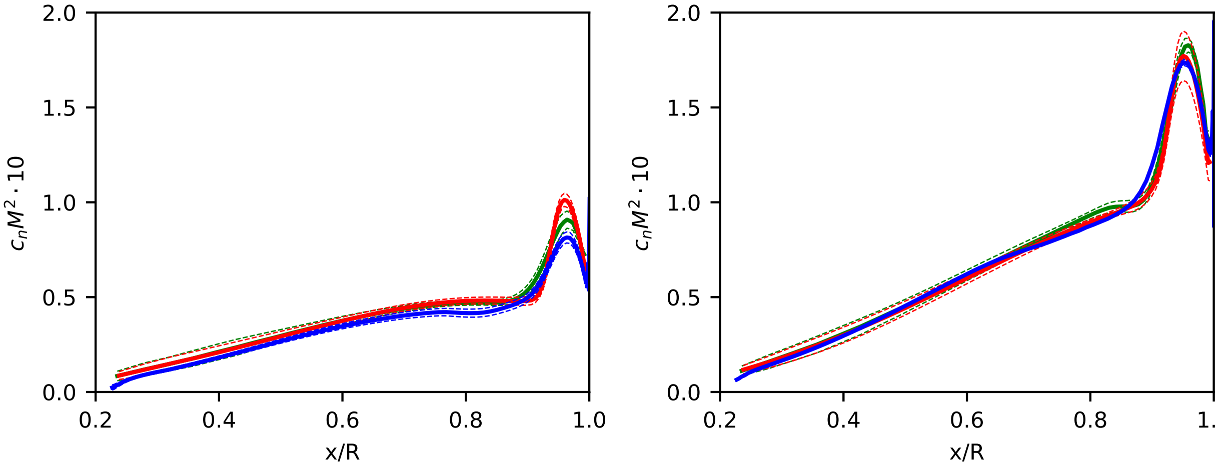

(a) $c_T/\sigma = 3.54/100$

(b) $c_T/\sigma = 6.37/100$

Figure 13: Normal force coefficients from the free simulations. The slim dashed lines show 2 standard deviations/95% interval added to the mean force with the thick line.

to a roughly matching thrust and potential minor variations were accepted in it, since the greater goal of the test run is to ensure a well operational rotor, actuation and instrumentation for the wind tunnel test along with refining the blade tracking. Thus, running the simulations at preset collective angles is preferred.

Not all simulations finished in time and some unexplained issues remain, however the underlying conclusion is that it is possible to carry out these simulations if sufficient amount of time is allocated. Increasing the accuracy through grid refinement and reducing time steps has also been observed. The general trend that the rotor could be safely operated at the lower thrust, but not at the nominal thrust was still captured by the simulations. The overall wall clock time of the simulations spanned over multiple months. With better parallized flow solvers and stronger time stepping approaches, this wall clock could have been reduced, however, the factor between free stream and boxed flow simulations will remain and somewhere between 50 and 100 revolutions are necessary to develop the boxed flow sufficiently. This number reduces with higher thrust as the induced velocities are higher. Estimating the required number of revolutions beforehand with the induced velocity according to momentum theory and a characteristic length will yield a fair cost estimate of the required physical time to be simulated.

Future recommendations for this kind of simulations would be:

1. Performing multiple simulations at fixed collective pitch angles and then interpolating the data onto the desired target thrusts will likely reduce the turn-around times for the boxed flow simulations. From the trimmed simulations in this paper, it was observed that oscillations occurred with the trim control angles, but due to the long convection times, quite some latency between input and reaction is given. It is likely an ill-posed control loop on the simulation side, which can simply be avoided if not further controlled.

2. Trimming the roll- and pitching moment is tertiary at best and therefore may be additionally neglected for single rotor simulations. Similarly, the effect of laminar-turbulent transition prediction is secondary when comparing boxed flow with out-of-ground hover.

3. If at hand, a fast Cartesian flow solver for the box grid is recommended. The assumption of a box proved to be viable enough for the test hall, despite some heavy-duty shelves and other apparati remaining in the pre-test hall during the experiment.

6 Aknowledgements

The lead author would like to thank the recently retired head of the DLR Institute of Aerodynamics and Flow technology, Christian-Cord Rossow, for granting extra HPC resources for these simulations.

References

[1] B. G. van der Wall, J. W. Lim, J. Riemenschneider, S. Kalow, G. Wilke, and D. D. Boyd, Jr., J. Bailly, Y. Delrieux, I. Cafarelli, Y. Tanabe, H. Sugawara, S. N. Jung, S. H. Hong, D.-H. Kim, H. J. Kang, G. Barakos, and R. Steininger, “Smart Twisting Active Rotor (STAR) - Pre-Test Predictions,” 48th European Rotorcraft Forum, September 2022.

[2] I. C. Cheeseman, and W. E. Bennett, “The effect of the ground on a helicopter rotor in forward flight,” Paper 3021, Aeronautical Research Council Reports & Memoranda, 1955.

[3] A. Graber, A. Rosen, A. and A. Seginer, “An investigation of a hovering rotor in ground effect,” *The Aeronautical Journal*, Vol. 95, (945), 1991, pp. 161–169. DOI: 10.1017/S0001924000023812

[4] W. Johnson, “Rotorcraft Aerodynamics Models for a Comprehensive Analysis,” 54th Annual Forum of the American Helicopters Society, May 1998.

[5] P.-M. Basset, O. Heuze, J. V. R. Prasad, and M. Hamers, “Finite State Rotor Induced Flow Model For Interferences and Ground Effect,” 57th Annual Forum of the American Helicopters Society, May 2001.

[6] S. Ananthan, J. G. Leishman, and M. Ramasamy, “The Role of Filament Stretching in the Free-Vortex Modeling of Rotor Wakes,” 58th Annual Forum and Technology Display of the American Helicopter Society, May 2002.

[7] J. K. Tritschler, M.Syal, R. Celi, and J. G. Leishman, “A Methodology for Rotorcraft Brownout Mitigation: Using Rotor Design Optimization,” American Helicopter Society 66th Forum, May 2010.

[8] T. R. Quackenbush, G. Whitehouse, B. S. Silbaugh, and P. V. Danilov, “Analysis of Rotor Configuration and Ground Proximity Effects on Hover Download,” Proceedings of the 74th Annual Forum, May 2018.

[9] D. T. Balch, and J. Lombardi, "Experimental study of main rotor tip geometry and tail rotor interactions in hover. Volume 1. Text and figures," Nasa contractor report 177336, Sikorsky Aircraft Stratford, CT, United States, 1985.

[10] P. E. Tanner, A. D. Overmeyer, L. N. Jenkins, C.-S. Yao, and Scott M. Bartram, "Experimental Investigation of Rotorcraft Outwash in Ground Effect," 71st American Helicopter Society Annual Forum, May 2015.

[11] G. Gibertini, D. Grassi, C. Parolini, D. Zagaglia and A. Zanotti, "Experimental investigation on the aerodynamic interaction between a helicopter and ground obstacles," *Proceedings of the Institution of Mechanical Engineers, Part G: Journal of Aerospace Engineering*, Vol. 229, (8), 2015, pp. 1395–1406. DOI: 10.1177/0954410014550501

[12] C. Schwarz, A. Bauknecht, C. C. Wolf, A. Coyle, and M. Raffel, "A Full-Scale Rotor-Wake Investigation of a Free-Flying Helicopter in Ground Effect Using BOS and PIV," *Journal of the American Helicopter Society*, Vol. 65, (3), 2020, pp. 1–20. DOI: doi:10.4050/JAHS.65.032007

[13] C. C. Wolf, A. Weiss, C. Schwarz, J. Braukmann, S. Koch, and M. Raffel, "Wake Unsteadiness and Tip Vortex System of Full-Scale Helicopters in Ground Effect," *Journal of the American Helicopter Society*, Vol. 67, (1), 2022, pp. 1–17. DOI: 10.4050/JAHS.67.012010

[14] B. M. Kutz, M. Kessler and E. Krämer, "Toolchain for Free Flight Measurement and Code Validation Purposes," 39th European Rotorcraft Forum, September 2013.

[15] B. M. Kutz, F. Bensing, M. Keßler, and E. Krämer, *CFD Calculation of a Helicopter Rotor Hovering in Ground Effect*, Springer Berlin Heidelberg, Berlin, Heidelberg, 2013, pp. 297–304. DOI: 10.1007/978-3-642-35680-3_36

[16] R. Boisard, "Aerodynamic investigation of a helicopter rotor hovering in the vicinity of a building," AHS International 74th Annual Forum & Technology Display, May 2018.

[17] S. Miesner, M. Keßler, E. Krämer, and U. Schäferlein, "Investigation of Near Ground Effects in Hover Flight for the Multi-Rotor Aircraft Volocopter-2X," Vertical Flight Society's 76th Annual Forum & Technology Display, October 2020.

[18] Y. Tanabe, H. Sugawara, S. Sunada, K. Yonezawa, and H. Tokutake, "Quadrotor Drone Hovering in Ground Effect," *Journal of Robotics and Mechatronics*, Vol. 33, (2), 2021, pp. 339–347. DOI: 10.20965/jrm.2021.p0339

[19] M. Sugiura, Y. Tanabe, H. Sugawara, K. Kimura, A. Oyama, M. Sato, K. Yoshikawa, Y. Buto, M. Kanazaki, Y. Kishi, D. Kikuchi, and T. Minajima, "Blade Shape Optimization of Mars Helicopter Exploring Pit Craters," 78th Annual Forum of the Vertical Flight Society, May 2022.

[20] K. Yoshikawa, Y. Buto, M. Sato, A. Oyama, M. Sugiura, Y. Tanabe, K. Kimura, K. Takekawa, Y. Kishi and M. Kanazaki, "Experimental Measurement and Numerical Simulation on Aerodynamic Characteristics of the rotor in Martian Helicopter," The Japan Society for Aeronautical and Space Sciences, 2022.

[21] Y. Tanabe, S. Saito, and H. Sugawara, "Validation of High Resolution CFD Analysis For Flowfield Around a Rotor," The 40th Japan Society for Aeronautical and SpaceSciences Annual Meeting, 2009.

[22] J. Raddatz, and J. K. Fassbender, "Block Structured Navier-Stokes Solver FLOWer," MEGAFLOW - Numerical Flow Simulation for Aircraft Design, edited by N. Kroll and J. K. Fassbender, 2005.

[23] K. Kitamura, and E. Shima, "Towards shock-stable and accurate hypersonic heating computations: A new pressure flux for AUSM-family schemes," *Journal of Computational Physics*, Vol. 245, 2013, pp. 62–83. DOI: 10.1016/j.jcp.2013.02.046

[24] S. Yamamoto, S. Kano, and H. Daiguji, "An Efficient CFD Approach for Simulating Unsteady Hypersonic Shock-Shock Interference Flows," *Computers & Fluids*, Vol. 27, (5), 1998, pp. 571–580. DOI: 10.1016/S0045-7930(97)00061-3

[25] G. Wilke, "Comparisons of Different Spatial Schemes and Limiters for Helicopter Flows," New Results in Numerical and Experimental Fluid Mechanics XIII, edited by A. Dillmann, G. Heller, E. Krämer, and C. Wagner, 2021. DOI: 10.1007/978-3-030-79561-0

[26] F. R. Menter, M. Kuntz, and R. Langtry , "Ten years of industrial experience with the SST turbulence model," *Heat and Mass Transfer*, Vol. 4, (1), 2003, pp. 625–633. DOI: 10.1.1.460.2814

[27] C. C. Heister, "A Method for Approximate Prediction of Laminar-Turbulent Transition on Helicopter Rotors," *Journal of the American Helicopter Society*, Vol. 63, (3), July 2018, pp. 1–14.

[28] S. Allmaras, F. T. Johnson, and P. Spalart, “Modifications and clarifications for the implementation of the Spalart-Allmaras turbulence model,” Seventh International Conference on Computational Fluid Dynamics (ICCFD7)„ January 2012.

[29] P. R. Spalart, S. Deck, M. Shur, K. D. Squires, M. Kh. Strelets, and A. Travin, “A New Version of Detached-eddy Simulation, Resistant to Ambiguous Grid Densities,” *Theoretical and Computational Fluid Dynamics*, Vol. 20, (3), May 2006, pp. 181. DOI: 10.1007/s00162-006-0015-0

[30] J. Dacles-Mariani, , G. G. Zilliac, J. S. Chow, and P. Bradshaw, “Numerical/experimental study of a wingtip vortex in the near field,” *AIAA Journal*, Vol. 33, (9), 1995, pp. 1561–1568. DOI: 10.2514/3.12826

[31] V. Vatsa, M. Carpenter, and D. Lockard, “Re-evaluation of an Optimized Second Order Backward Difference (BDF2OPT) Scheme for Unsteady Flow Applications,” 48th AIAA Aerospace Sciences Meeting Including the New Horizons Forum and Aerospace Exposition, 2010. DOI: 10.2514/6.2010-122

[32] B. Benoit, A.-M. Dequin, K. Kampa, W. von Grünhagen, P.-M. Basset, and B. Gimonet, “HOST, a General Helicopter Simulation Tool for Germany and France,” 56th Annual Forum of the American Helicopters Society, May 2000.